

Synthesis of novel phthalimide-based piperazine conjugated analogs as anti-malarial agents

Meenakshi Bansal,^{1,2} Sumit Kumar,^{1*} Brijesh Rathi^{2*}

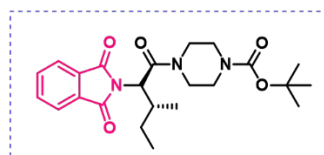
¹Department of Chemistry, Deenbandhu Chhotu Ram, University of Science & Technology, Murthal, Sonapat Haryana 131039 India.

²Laboratory for Translational Chemistry and Drug Discovery, Department of Chemistry, Hansraj College, University of Delhi, Delhi-110007 India

Submitted on: 22-Jun-2023, Accepted and Published on: 07-Aug-2023

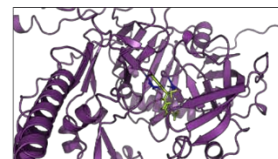
Article

ABSTRACT

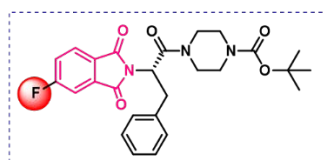


IC₅₀ (μM) at 48h (6d) = 1.20 ± 0.02

Plm_IX-6d Complex

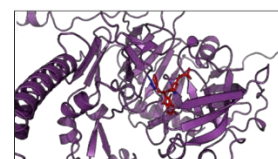


In the present report, we synthesized twelve novel phthalimide analogs and evaluated for antiplasmodial efficacy on *Plasmodium falciparum* culture. Two molecules exhibited significant inhibition percentages at 1 μM concentration without any apparent cytotoxicity on HepG2 cells. Inhibitory concentration (IC₅₀) for both the hit compounds 6d and 8a was observed in micromolar range, 1.20 μM and 1.66 μM, respectively. Extensive in silico studies conducted indicate plasmepsin IX as a possible target for inhibitory activity of the reported molecules.



IC₅₀ (μM) at 48h (8a) = 1.66 ± 0.03

Plm_IX-8a Complex



In the present report, we synthesized twelve novel phthalimide analogs and evaluated for antiplasmodial efficacy on *Plasmodium falciparum* culture. Two molecules exhibited significant inhibition percentages at 1 μM concentration without any apparent cytotoxicity on HepG2 cells. Inhibitory concentration (IC₅₀) for both the hit compounds 6d and 8a was observed in micromolar range, 1.20 μM and 1.66 μM, respectively. Extensive in silico studies conducted indicate plasmepsin IX as a possible target for inhibitory activity of the reported molecules.

Keywords: Phthalimide; Amino acid linker; Piperazine; *Plasmodium falciparum*; Molecular docking

INTRODUCTION

Malaria continues to be the most prevalent and lethal vector-borne devastating cause of death in tropical geographies, with a significant portion of the population still depending on the utilization of medicinal plants to combat the pathogenicity of the disease.^{1,2} Malaria is usually caused by protozoan parasites from the *Plasmodium* genus, which invade the human host's erythrocytes (red blood cells). *Plasmodium* has five different types that can attack people: *P. falciparum*, *P. vivax*, *P. ovale*, *P. malariae*, and *P. knowlesi*. Among the five plasmodial species that pose the most threat is *P. falciparum*, accounting for 90% of fatal disease cases.^{3,4} As per the latest World Malaria Report 2022, a total of 247 million cases in 84 malaria-endemic countries were reported in 2022.⁵⁻⁷ In African region, the vast majority of malaria cases, specifically 99.7%, were attributed to *P. falciparum*, with a disproportionate number of those targeted

being children and pregnant women. Although, the number of people associated with the disease has gone down in recent years, there is an urgent need to achieve the eradication by novel treatment options.

Targeting various phases of the complex *P. falciparum* life cycle (*i.e.*, asexual replication in the host's bloodstream and sexual reproduction in the mosquito vector) will probably be crucial for eradicating this pathogen.⁸ Most therapeutics effective on asexual blood stage that is clinically significant and responsible for causing the disease.⁹ The efficacy of effective drugs, including chloroquine and quinine, has been decreasing due to the emergence of resistance.^{10,11} Artemisinin-based combination treatment (ACT) options are widely used to treat malaria. The efficacy of artemisinin in current drug combinations is attributed to its activity against a wide range of drug-resistant strains.¹² Nevertheless, there has been a concerning increase in the resistance of parasites to artemisinin and the accompanying drugs employed in the present standard treatment approach. It necessitates the discovery of novel pharmaceuticals utilizing innovative mechanisms of action.^{13,14}

Scaffolds based on phthalimide (Pht) were developed based on our previous research conducted in our lab, which have shown promising results against malaria parasite.¹⁵⁻¹⁹ Besides, Pht and its derivatives are highly valued in medicinal chemistry, serving

*Corresponding Author: Dr. Sumit Kumar, Ph.D. and Dr. Brijesh Rathi, PhD
Email: sumitmalik.chem@dcrstm.org (SK), brijeshrathi@hrc.du.ac.in (BR)



as valuable scaffolds and pharmacophores for advancing new therapeutics against various diseases.²⁰⁻²² Figure 1 highlights the importance of scaffolds known in the literature as having good efficacy against *Pf3D7* strain of malaria parasite.^{19,22-25} The present study involves further structural modifications of previously reported Pht based antiplasmodial hits.¹⁶ These modifications are based on amide linkages that utilize Pht as a parent scaffold and amino acids as a complimentary scaffold, as they possess the potential to serve as drug synthons.²⁶ Further, heterocyclic moieties *i.e.*, piperazines and cyclic amines, are significant constituents in synthesizing substituted amide linkages.^{27,28,29} Consistent with previously published data, certain analogs featuring C₂ symmetry with piperazine have exhibited better outcomes.¹⁶ In this study, we were curious to know the role of C₂ symmetry on the antiplasmodial activity. Therefore, we synthesized twelve novel compounds without any C₂ symmetry and evaluated their efficacy on *Pf3d7* strain in cell culture.

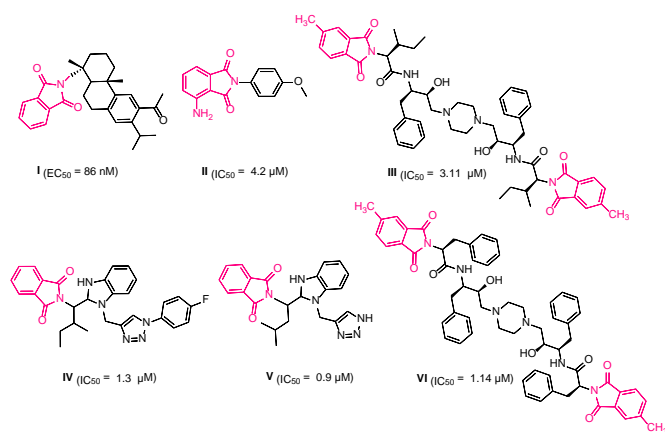


Figure 1. Examples of Pht based inhibitors showing efficacy against *Plasmodium falciparum*.

EXPERIMENTAL

Chemistry

Material: The solvents and reagents used in the investigation were procured from the commercial sources and employed without any purification process. The homogeneity and purity of all products were evaluated using thin-layer chromatography (TLC) on alumina-coated plates (Merck). The experiment involves applying product samples dissolved in chloroform (CHCl₃) were loaded on TLC plates, which were subsequently subjected to development in Ethyl acetate/Petroleum ether (1:1, v/v). Upon detection of minor impurities through iodine vapour/UV light visualization, the compounds underwent additional purification *via*. Flash column chromatography (Yamazen, Japan) utilizing alumina gel columns (100-200 mesh size, Biotage). The determination of melting points was carried out on BUCHI Melting Point M-560. The ¹H and ¹³C Nuclear Magnetic Resonance (NMR) spectra were acquired on a JEOL ECX-400P instrument at 400 MHz and 100 MHz, respectively, in CDCl₃ solvent at the University of Delhi's USIC facility. The Agilent Technology-6530, Accurate mass, Q-TOF LCMS

spectrometer located at USIC, University of Delhi was used to acquire the high-resolution mass spectral (HRMS) data.

General procedure for synthesis: Synthesis of Pht-piperazine analogs already been optimized in our lab.^{16,17} Similar methods were followed to synthesize all the listed Pht compounds **6-8(a-d)** in this manuscript. In the beginning, substituted phthalic anhydrides **1a-c** (1.0 equiv; 5.0 mmol) and different amino acids **2a-d** (1.0 equiv; 5.0 mmol) were taken in toluene and refluxed at 120 °C for 2 h in presence of trimethylamine (TEA, 0.1 equiv; 0.5 mmol). After completion, the reaction mixture was extraction ethyl acetate and water. The resulting organic layer was subsequently collected and subjected to drying using anhydrous sodium sulphate. Next, excess ethyl acetate was removed under reduced vacuum pressure to afford intermediate *N*-phthaloyl-L-amino acids, **3-5(a-d)**, and used in the next step without any purification. Further, intermediates **3-5(a-d)** (1.0 equiv, 2.0 mmol) were coupled with Boc-protected piperazine (1.0 equiv, 2.0 mmol), which were taken in the round bottom (RB) flask and dissolved in dichloromethane (DCM), followed by dropwise addition of TEA (3 equiv; 6.0 mmol) to the reaction mixture. After 20 mins, EDC·HCl (2.0 equiv., 4.0 mmol) was introduced to the reaction mixture, followed by the subsequent addition of HOBt (2.0 equiv, 4.0 mmol) after the next 20 mins. After a 30-minutes of stirring, the Boc-protected piperazine compound was gradually introduced into the reaction vessel. Before this addition, the compound was dissolved in dichloromethane (DCM) within a separate round-bottom flask (RB flask). All the additions were conducted at a temperature 0 °C followed by stirring at ambient temperature for a duration of 24 h. Lastly, the excess of the solvent was eliminated using rotary evaporator. Subsequently, the resulting mixture was extracted using ethyl acetate and water. The acquired organic layer was collected, dehydrated using anhydrous sodium sulphate, and concentrated using a rotavapor. The crude products **6-8(a-d)** underwent further purification *via*. flash column chromatography using a solvent system consisting of ethyl acetate and hexane at 2:8 (v/v). The spectroscopic techniques *i.e.*, NMR (¹H & ¹³C) and HRMS, confirmed the chemical composition of the synthesized compounds (Figure S1-S50).

Spectroscopic data

tert-Butyl (S)-4-(2-(1,3-dioxoisindolin-2-yl)-3-phenylpropanoyl)piperazine-1-carboxylate (**6a**)

White solid; yield 78%; m.p. 165-167 °C. ¹H-NMR (400 MHz, CDCl₃) δ 7.74 (dd, *J* = 5.5, 3.4 Hz, 2H), 7.52 (dd, *J* for = 5.5, 3.4 Hz, 2H), 7.19 – 7.04 (m, 5H), 5.32 (t, *J* = 7.9 Hz, 1H), 3.71 – 3.32 (m, 8H), 3.30 – 3.04 (m, 2H), 1.46 (s, 9H). ¹³C NMR (100 MHz, CDCl₃) δ 168.3, 166.6, 155.0, 137.3, 133.2, 132.3, 129.6, 129.1, 127.4, 125.3, 81.0, 56.7, 45.0, 43.5, 37.3, 28.4.

tert-Butyl (S)-4-(2-(1,3-dioxoisindolin-2-yl)-3-methylbutanoyl)piperazine-1-carboxylate (**6b**)

White solid; yield 76%; m.p. 143-145 °C. ¹H NMR (400 MHz, CHLOROFORM-D) δ 7.85 (dd, *J* = 5.4, 3.0 Hz, 2H), 7.74 (dd, *J* = 5.5, 3.1 Hz, 2H), 4.63 (d, *J* = 10.2 Hz, 1H), 3.68 – 3.09 (m, 9H), 1.76 (s, 1H), 1.42 (s, 9H), 1.04 (d, *J* = 6.6 Hz, 3H), 0.87 (d, *J* = 6.8 Hz, 3H). ¹³C NMR (100 MHz, CDCl₃) δ 167.8, 166.9, 154.5,

134.5, 131.3, 123.7, 80.4, 56.3, 45.6, 42.3, 28.4, 27.6, 20.6, 19.2. HRMS calcd. (M+H) for C₂₂H₃₀N₃O₅ 416.2141; found 416.2172.

tert-Butyl (S)-4-(2-(1,3-dioxoisindolin-2-yl)-4-methylpentanoyl)piperazine-1-carboxylate (6c)

White solid; yield 74%; m.p. 146-148 °C. ¹H NMR (400 MHz, CDCl₃) δ 7.87–7.82 (m, 2H), 7.76–7.69 (m, 2H), 5.13 (dd, *J* = 11.3, 4.4 Hz, 1H), 3.39 (d, *J* = 22.2 Hz, 8H), 1.60 (m, 2H), 1.44 (s, 9H), 0.95 (t, *J* = 6.9 Hz, 7H). ¹³C NMR (100 MHz, CDCl₃) δ 168.2, 134.4, 131.7, 123.6, 80.5, 50.00, 37.4, 28.5, 25.3, 23.2, 21.4. HRMS calcd. (M+H) for C₂₃H₃₂N₃O₅ 430.2297; found 430.2329.

tert-Butyl 4-((2S,3R)-2-(1,3-dioxoisindolin-2-yl)-3-methylpentanoyl) piperazine-1-carboxylate (6d)

White solid; yield 72%; m.p. 173-175 °C. ¹H NMR (400 MHz, CDCl₃) δ 7.85–7.81 (m), 7.74–7.71 (m), 4.72 (dd, *J* = 13.1, 10.3 Hz), 3.70–3.16 (m), 2.90 (d, *J* = 31.6 Hz), 1.41 (s), 0.96 (dd, *J* = 13.9, 6.9 Hz), 0.86–0.81 (m). ¹³C NMR (100 MHz, CDCl₃) δ 167.90, 167.29, 154.55 (s), 134.5, 131.4, 124.0, 123.7, 80.4, 55.1, 54.9, 45.7, 45.5, 42.3, 29.8, 28.4, 27.2, 25.4, 16.6, 15.2, 11.5, 10.7. HRMS calcd. (M+H) for C₂₃H₃₂N₃O₅ 430.2297; found 430.2327.

tert-Butyl (S)-4-(2-(5-methyl-1,3-dioxoisindolin-2-yl)-3-phenylpropanoyl)piperazine-1-carboxylate (7a)

White solid; yield 76%; m.p. 154-156 °C. ¹H NMR (400 MHz, CDCl₃) δ 7.64 (d, *J* = 7.6 Hz, 1H), 7.56 (s, 1H), 7.46 (d, *J* = 7.7 Hz, 1H), 7.21–7.10 (m, 5H), 5.21 (dd, *J* = 9.4, 6.3 Hz, 1H), 3.66–3.10 (m, 10H), 2.47 (s, 3H), 1.40 (s, 9H). ¹³C NMR (100 MHz, CDCl₃) δ 167.7, 167.2, 145.7, 137.0, 134.9, 131.7, 129.3, 28.6, 127.0, 124.2, 123.5, 80.4, 52.4, 35.4, 28.4, 22.1.

tert-Butyl (S)-4-(3-methyl-2-(5-methyl-1,3-dioxoisindolin-2-yl)butanoyl)piperazine-1-carboxylate (7b)

White solid; yield 78%; m.p. 136-138 °C. ¹H NMR (400 MHz, CDCl₃) δ 7.70 (d, *J* = 7.6 Hz, 1H), 7.62 (s, 1H), 7.50 (d, *J* = 5.6 Hz, 1H), 4.58 (d, *J* = 10.1 Hz, 1H), 3.73–2.95 (m, 9H), 2.49 (s, 3H), 1.40 (s, 9H), 1.02 (d, *J* = 6.6 Hz, 3H), 0.83 (d, *J* = 6.8 Hz, 3H). ¹³C NMR (100 MHz, CDCl₃) δ 168.0, 166.9, 145.9, 135.0, 131.7, 128.7, 124.2, 123.6, 80.44, 56.1, 45.5, 42.3, 28.4, 22.1, 20.7, 19.1.

tert-Butyl (S)-4-(4-methyl-2-(5-methyl-1,3-dioxoisindolin-2-yl)pentanoyl)piperazine-1-carboxylate (7c)

White solid; yield 72%; m.p. 117-119 °C. ¹H NMR (400 MHz, CDCl₃) δ 7.68 (d, *J* = 1.4 Hz, 1H), 7.61 (d, *J* = 7.5 Hz, 1H), 7.29 (dd, *J* = 7.5, 1.4 Hz, 1H), 4.84 (t, *J* = 7.3 Hz, 1H), 3.65–3.11 (m, 8H), 2.20 (s, 3H), 1.88–1.55 (m, 2H), 1.40–1.32 (m, 10H), 0.88 (d, *J* = 6.3 Hz, 6H). ¹³C NMR (100 MHz, CDCl₃) δ 167.9, 167.2, 154.5, 146.3, 133.7, 132.5, 130.8, 124.4, 124.1, 80.5, 52.0, 44.5, 43.0, 39.5, 27.9, 25.1, 22.6, 20.9.

tert-Butyl 4-((2S,3R)-3-methyl-2-(5-methyl-1,3-dioxoisindolin-2-yl)pentanoyl)piperazine-1-carboxylate (7d)

White solid; yield 72%; m.p. 167-169 °C. ¹H NMR (400 MHz, CDCl₃) δ 7.70 (d, *J* = 1.4 Hz, 1H), 7.56 (d, *J* = 7.5 Hz, 1H), 7.28 (dd, *J* = 7.5, 1.4 Hz, 1H), 3.96 (d, *J* = 3.8 Hz, 1H), 3.45 (m, 8H), 2.47–2.42 (m, 1H), 2.22 (s, 3H), 1.36 (s, 9H), 1.20–1.13 (m, 2H), 0.92 (d, *J* = 6.6 Hz, 3H), 0.85 (t, *J* = 6.7 Hz, 3H). ¹³C NMR (100 MHz, CDCl₃) δ 168.1, 164.8, 152.0, 143.8, 131.2, 130.0,

128.3, 121.9, 121.6, 78.0, 54.2, 42.0, 40.5, 31.1, 25.4, 22.5, 18.4, 13.4, 8.6.

tert-Butyl (S)-4-(2-(5-fluoro-1,3-dioxoisindolin-2-yl)-3-phenylpropanoyl)piperazine-1-carboxylate (8a)

White solid; yield 75%; m.p. 141-143 °C. ¹H NMR (400 MHz, CDCl₃) δ 7.77 (dd, *J* = 8.2, 4.4 Hz, 1H), 7.44 (dd, *J* = 7.0, 2.2 Hz, 1H), 7.38–7.30 (m), 7.27–7.11 (m, 5H), 5.30–5.19 (m, 1H), 3.65–3.54 (m), 3.50–3.44 (m, 2H), 3.37–3.23 (m, 3H), 1.41 (s, 9H). ¹³C NMR (100 MHz, CDCl₃) δ 167.8, 167.0, 165.9 (d, *J* = 254.8 Hz), 154.4, 136.7, 134.2 (d, *J* = 9.6 Hz), 129.2, 128.7, 127.2, 126.0 (d, *J* = 9.7 Hz), 121.4 (d, *J* = 23.8 Hz) 111.3, 80.5, 52.9, 50.9, 35.1, 28.4.

tert-Butyl (S)-4-(2-(5-fluoro-1,3-dioxoisindolin-2-yl)-3-methylbutanoyl) piperazine-1-carboxylate (8b)

White solid; yield 64%; m.p. 164-166 °C. ¹H NMR (400 MHz, CDCl₃) δ 7.75 (dd, *J* = 7.5, 5.1 Hz, 1H), 7.62 (dd, *J* = 5.6, 2.3 Hz, 1H), 7.29–7.20 (m, 1H), 4.04 (d, *J* = 3.5 Hz, 1H), 3.75–3.33 (m, 8H), 2.69–2.62 (m, 1H), 1.44 (s, 9H), 1.02 (d, *J* = 6.4 Hz, 6H). ¹³C NMR (100 MHz, CDCl₃) δ 167.3, 166.8, 166.1 (d, *J* = 254.3 Hz), 154.5, 133.18 (d, *J* = 7.6 Hz), 128.6 (d, *J* = 4.7 Hz), 126.1 (d, *J* = 6.7 Hz), 120.1 (d, *J* = 27.7 Hz), 113.6 (d, *J* = 26.7 Hz), 80.4, 58.6, 44.4, 43.0, 27.8, 28.2, 18.8.

tert-Butyl (S)-4-(2-(5-fluoro-1,3-dioxoisindolin-2-yl)-4-methylpentanoyl)piperazine-1-carboxylate (8c)

White solid; yield 65%; m.p. 178-180 °C. ¹H NMR (400 MHz, CDCl₃) δ 7.74 (dd, *J* = 7.5, 5.0 Hz, 1H), 7.65 (dd, *J* = 8.0, 1.5 Hz, 1H), 7.28–7.24 (m, 1H), 4.94 (t, *J* = 7.3 Hz, 1H), 3.70–3.28 (m, 8H), 1.97–1.64 (m, 2H), 1.50–1.44 (m, 1H), 1.42 (s, 9H), 0.97 (d, *J* = 6.2 Hz, 6H). ¹³C NMR (100 MHz, CDCl₃) δ 168.4, 168.0, 167.2 (d, *J* = 253.4 Hz), 133.3 (d, *J* = 7.8 Hz), 128.7 (d, *J* = 4.8 Hz), 126.2 (d, *J* = 6.6 Hz), 120.2 (d, *J* = 27.5 Hz), 113.7 (d, *J* = 26.6 Hz), 80.5, 52.0, 44.5, 43.1, 39.5, 28.0, 25.2, 22.7.

tert-Butyl 4-((2S,3R)-2-(5-fluoro-1,3-dioxoisindolin-2-yl)-3-methylpentanoyl)piperazine-1-carboxylate (8d)

White solid; yield 68%; m.p. 153-155 °C. ¹H NMR (400 MHz, CDCl₃) δ 7.78 (dd, *J* = 7.5, 5.1 Hz, 1H), 7.56 (dd, *J* = 8.1, 1.4 Hz, 1H), 7.26–7.20 (m, 1H), 4.03 (d, *J* = 4.9 Hz, 1H), 3.71–3.39 (m, 8H), 2.41–2.30 (m, 1H), 1.43 (s, 9H), 1.32–1.23 (m, 2H), 1.04–0.89 (m, 6H). ¹³C NMR (100 MHz, CDCl₃) δ 168.1, 167.0, 166.6 (d, *J* = 253.9 Hz), 133.0 (d, *J* = 7.6 Hz), 128.3 (d, *J* = 4.7 Hz), 125.9 (d, *J* = 6.7 Hz), 119.8 (d, *J* = 27.7 Hz), 113.4 (d, *J* = 26.7 Hz), 80.2, 56.4, 44.2, 42.7, 33.3, 27.6, 24.7, 15.7, 10.6.

Biological evaluation

In vitro cytotoxicity assay: MTT assay was performed to test cytotoxicity on HepG2 cells. The HepG2 cells were cultured in flasks using Dulbecco's Modified Eagle Medium (DMEM) supplemented with 10% fetal bovine serum (FBS) and gentamicin. The cells were maintained at a temperature of 37 °C and a carbon dioxide (CO₂) concentration of 5%. The medium was refreshed three times per week. Subsequently, the cells underwent trypsinization, followed by a thorough washing process. They were then suspended in a complete medium and subsequently distributed onto 96-well plates, with each well containing 5000 cells. The plates were then incubated at a temperature of 37 °C for a duration of 24 hours. Following a 48-

hour incubation period, the supernatant was extracted, and a volume of 100 μL of MTS solution in complete DMEM was introduced into each well. The plates were then incubated for 2 hours at 37 $^{\circ}\text{C}$, then analyzed using a spectrophotometer using a predetermined absorbance value of 450 nm. The obtained data were analyzed in Excel to evaluate cytotoxicity.

Parasite culture (SYBR Green assay): The development of *Pf3D7* was achieved by implementing the methodologies described by Trager and Jensen.³⁰ Parasites were cultured using human O+ red blood cells in a complete medium of RPMI 1640 supplemented with NaHCO_3 , AlbuMax II, hypoxanthine, and gentamicin. The parasites were cultivated in a gaseous environment consisting of 5% oxygen, 5% carbon dioxide, and 90% nitrogen while maintaining a temperature of 37 $^{\circ}\text{C}$. SYBR Giemsa-stained blood smears were evaluated to ascertain the presence of parasites. The compounds' clinical efficacy was assessed against *Pf3D7* at various doses by measuring fluorescence using a multimode microplate reader in a lightless environment. All the experiments were performed in triplicate.

Hemolysis: The experiment on hemolysis was performed using a 10% (v/v) suspension of red blood cells (RBCs). Before the assay, RBCs underwent a washing procedure using phosphate-buffered saline (PBS) with a pH of 7.4, followed by a subsequent resuspension in PBS. Subsequently, the erythrocytes were subjected to varying concentrations of compounds for a duration of 2 hours at a temperature of 37 $^{\circ}\text{C}$. After undergoing the treatment, the samples were subjected to centrifugation at a speed of 800 revolutions per minute for 5 minutes, while being kept at the ambient temperature. The aqueous component of the specimen was collected and underwent spectrophotometric evaluation at a wavelength of 540 nm to determine the extent of erythrocyte lysis. All the experiments were performed in triplicate.

In silico studies

The ADME profile of the synthesized compounds was calculated using SWISS ADME³¹ and Molsoft L.L.C.³² The anticipated ADME characteristics involve various parameters as represented in Table S1; supporting information. Target proteins were optimized and cleaned up before molecular docking studies were conducted. Schrödinger (Schrödinger Release 2021-1) software was used for all the processes *i.e.*, protein purification, ligand preparation, molecular docking, and binding free energy calculation, as detailed in our previously published research.^{33, 34}

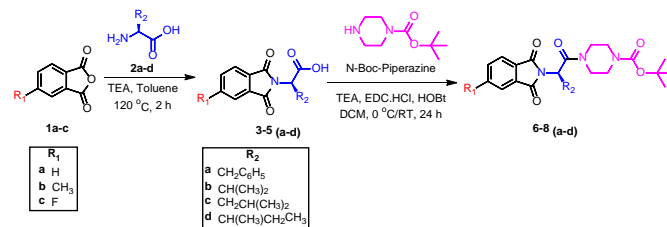
RESULT AND DISCUSSION

Chemistry: Synthesis and characterization

Previously, our group synthesized C_2 symmetric based inhibitor, which displayed good activity against malaria parasites.^{22, 24} The top hits among C_2 symmetric analogs showed IC_{50} of 1.14 μM (Figure 1) against *Pf3D7* strain of malaria parasite. Therefore, here we were curious to get an insight into the role of C_2 symmetry by synthesizing twelve novel molecules without any associated symmetry as shown in Scheme 1.

Initially, synthetic procedure began with the sublimation reaction of substituted phthalic anhydrides **1a-c** with amino acids **2a-d** was carried out to obtain the intermediate phthaloyls **3-5(a-d)**

d), which were further coupled with *N*-Boc-piperazine to yield the final products **6-8(a-d)** as depicted in Scheme 1. Structural modifications were performed on substitution with methyl and fluorine group on the aromatic ring to explore the possible variations with Pht moiety. The synthesized compounds were confirmed by characterization (^1H & ^{13}C) NMR and HRMS.



Scheme 1. Synthesis of twelve Pht analogs.

Biology

Cytotoxicity evaluation: At first, an MTT experiment was done on the HepG2 cell line to test the viability of synthesized Pht analogs. Figure 2 shows that the chemicals were tested at three different concentrations: 10, 100, and 500 μM . Up to 500 μM concentration, it was clear that none of the compounds harmed cells. So, all of the substances were deemed safe to more biological assays.

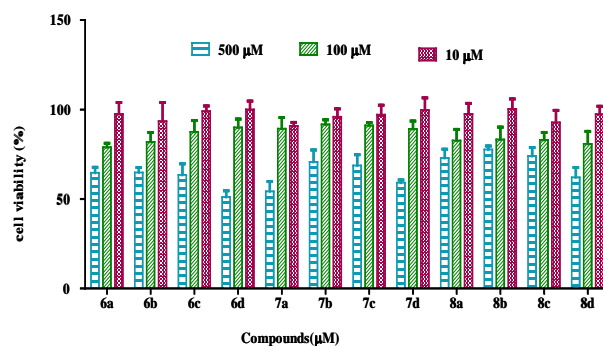


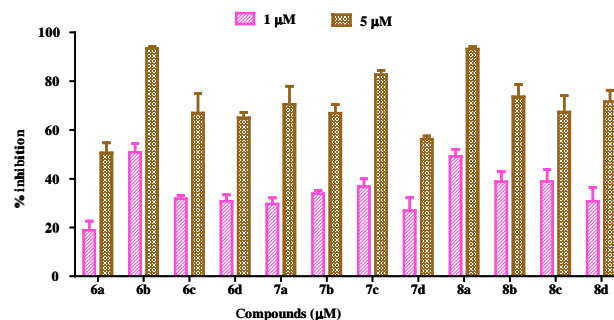
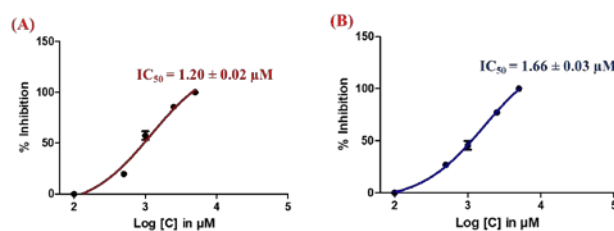
Figure 2. Cytotoxicity evaluated on HepG2 cell line at three different concentrations *i.e.*, 10, 100, and 500 μM .

Antiplasmodial and hemolytic activity: A preliminary assessment was carried out to evaluate antiplasmodial activity of newly synthesized Pht analogs towards *Pf* culture. Two distinct concentrations, 1 μM and 5 μM , of all the compounds were treated to the CQ-sensitive strain *Pf3D7*. The results indicated that all the listed compounds exhibited $\sim 50\%$ inhibition of the parasite at 5 μM concentration. The listed compounds displayed noteworthy antiplasmodial activity, as indicated in Figure 3 and Table 1. Interestingly, two compounds, **6d** and **8a** showed 51% and 49% inhibitory activity at 1 μM , respectively.

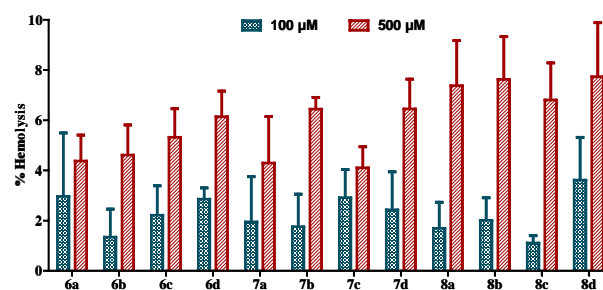
Further, based on initial screening, hit compounds **6d** and **8a** were selected for their 50% inhibitory concentration (IC_{50}) determination, as depicted in Figure 4. The IC_{50} indicated that both compounds **6d** and **8a** showed low micromolar efficacy against *Pf3D7* strain with IC_{50} values of 1.20 μM and 1.66 μM , respectively.

Table 1. Table representing *in vitro* antiplasmodial activity for synthesized analogs **6-8(a-d)** against *Pf3D7* strain.

Entry No.	Comp. Code	Structure	% inhibition against <i>Pf3D7</i> strain	
			1 μM	5 μM
1.	6a		19	51
2.	6b		31	65
3.	6c		32	67
4.	6d		51	93
5.	7a		30	70
6.	7b		34	67
7.	7c		37	83
8.	7d		27	56
9.	8a		49	92
10.	8b		39	73
11.	8c		39	67
12.	8d		31	72

**Figure 3.** The percentage inhibition of all synthesized Pht analogs against *Pf3D7* at two different concentrations (1 μM and 5 μM).**Figure 4.** Graphical representation of IC_{50} determination curves for A) compound **6d**; and B) compound **8a** against *Pf3D7* strain among Pht and Boc-piperazine-based compounds.

As such antimalarial compounds are known to selectively target *Plasmodium* parasites during their intra-erythrocytic stage and should not damage RBCs.³⁵ Consequently, a hemolytic assay was conducted on RBC suspension [10% (v/v)] that had been subjected to two distinct concentrations (*i.e.*, 100 and 500 μM) of all the compounds. The degree of hemolysis was quantified at wavelength of 500 nm, as illustrated in Figure 5. The results indicate that hemolysis does not occur significantly in RBCs upto 500 μM concentration.

**Figure 5.** Effect of compounds on human RBCs at 100 and 500 μM concentration.

Next, structure-activity relationship (SAR) analysis was conducted using the OSIRIS Data Warrior V 5.2.1 software (Figure 6), which is available for download from <http://www.openmolecules.org>. The programme created the SALI matrix to facilitate the study of twelve Pht analogs. Figure 6 shows antiplasmodial activity at 1 μM against *Pf3D7* strain and % hemolysis at 500 μM . **6a-6d** have no phthalic moiety replacement, **7a-7d** have methyl substitution, and **8a-8d** have fluoro substitution. The % inhibition (19-51% of all chemicals)

and % hemolysis are shown here in different colors and shapes. As indicated in Figure 6, compound **6a** (19%) has the lowest % inhibition at 1 μ M against *Pf3D7* strain with no phthalic substitution and phenylalanine as an amino acid linker. However, **7a** (methyl substitution) inhibited 30% and **8a** (fluoro substitution) 49% of the parasite, by substituting **6b** with a valine amino acid linker enhanced % inhibition from 31% to 34% (**7b**) and 37% (**8b**). Compound **6c** with leucine as an amino acid linker demonstrated 32% inhibition, whereas **7c** (37% inhibition, methyl substitution) and **8c** (39% inhibition, fluoro substitution) showed no improvement owing to phthalic group replacement. Next, compound **6d** with no phthalic substitution and *iso*-leucine as an amino acid linker inhibited 51% of the parasite. **8d** (fluoro substitution) had 31% inhibition and **7d** (methyl substitution) 27%. All substances demonstrated comparable hemolysis at 500 μ M.

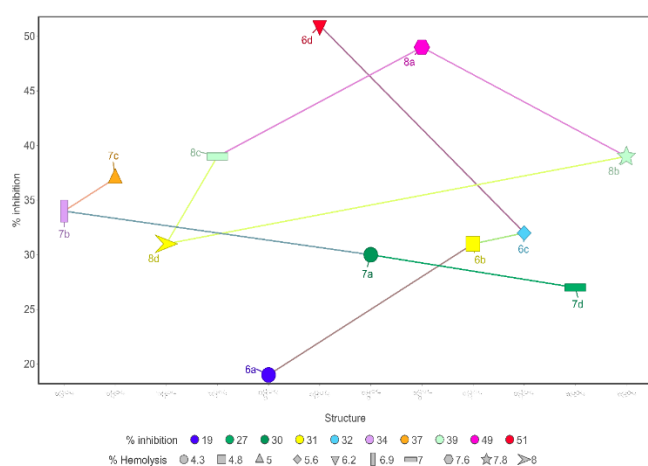


Figure 6. Structure-activity Relationship (SAR) using the OSIRIS Data Warrior V 5.2.1 software.

Computational studies

All of the molecules had good physiochemical qualities that are needed for the development of a drug molecule, as shown by the data in Table S1; supporting information. The evaluated compounds underwent an assessment for their Drug-likeness model score, which ranges from -2 to +2 and indicates drugability. The Blood-Brain Barrier (BBB) score was also determined, with 0 showing a low value and 6 showing a very high value. According to Weaver *et al.*,³² maintaining an optimal value of the BBB can protect the brain against the harmful side effects of therapeutic agents. Simultaneously, pharmaceuticals designed for neurological disorders must penetrate BBB at efficacious levels. Consequently, the examination of the interaction between BBB and specially designed therapeutic agents has the potential to yield significant and effective drug development. Each of the synthesized compounds exhibited an optimal score for BBB permeability, as none demonstrated a value below 2 or above 3. This suggests that the compounds are unlikely to cause harm to the brain. All of the chemical compounds outlined in this study exhibited favorable parameters and did not demonstrate any Lipinski violations.

Next, a comprehensive set of 62 proteins, accompanied by their respective accession numbers, were obtained from the Uniprot database (Accessed on 15 May 2023). The essentiality of these proteins was further investigated in Plasmodb. A total of 19 essential proteins were examined, two proteins, namely Subtilisin-like protease 1 and 2, were identified as substrates and subsequently excluded from further analysis. A comprehensive analysis revealed that a subset of 17 genes out of 60 were identified as essential, as indicated in Table S2 and Figure S28; supporting information. The amino acid residues of the 17 proteins were subsequently examined in order to determine the presence of any analogous protein in human. Only those that exhibited a percentage of identical residues below 30.0% were chosen to eliminate the possibility of proteins with similar characteristics.³⁶ Additionally, proteins with a query coverage below 55% were also included.³⁷ Four proteins were excluded from the analysis based on their structural similarity, leaving a remaining set of 13 proteins that were subsequently investigated for their structural availability. This investigation examined whether crystal structures or protein models generated by α -fold were accessible for these 13 proteins. Except for Eukaryotic translation initiation factor 2- α kinase PK4 (Uniprot accession no. C6KTB8), for which no structural information was available, structures were obtained for the remaining 12 proteins and are listed in Table 2.

Next, molecular docking was conducted to investigate the binding affinity of both identified hits, **6d** and **8a**, with 12 proteins, as outlined in Table 2. The obtained results were additionally validated through blind docking. The compounds **6d** and **8a** exhibited most affinity for Plm IX, as indicated by their respective docking scores of -5.001 and -5.322 Kcal/mol (Table 2, Figure 7). Both compounds exhibited comparable affinity scores, indicating no statistically significant difference, which was consistent with the wet lab experimental results. The obtained results were additionally validated through blind docking experiments, which revealed that compounds **6d** and **8a** exhibited interactions with DNA endonuclease, serine repeat antigen protein 5, as well as PlmIX (Figure 7 and 8). However, the most excellent affinity was observed exclusively for PlmIX, as indicated in Table 2. Our finding indicated that Plm IX could be the possible target protein for both the compounds, however, further validation studies are essential before reaching any conclusion.

Table 2. Site specific docking and blind docking results.

S. No.	Title	Docking score (Kcal/mol)	XP Gscore (Kcal/mol)	MMGB SA dG Bind (Kcal/mol)	Blind Docking
1.	Calcium-dependent protein kinase 5				
2.	6d	-3.574	-3.574	-42.71	Fail
3.	8a	-3.04	-3.04	-43.77	Fail

4.	Ubiquitin carboxyl-terminal hydrolase UCH54				
5.	6d	-3.061	-3.061	-53.84	Fail
6.	8a	-2.427	-2.427	-51.03	Fail
7.	Ubiquitin carboxyl-terminal hydrolase UCH54				
8.	6d	-4.01	-4.01	-50.13	Fail
9.	8a	-3.81	-3.81	-41.85	Fail
10.	Bifunctional glucose-6-phosphate 1-dehydrogenase/6-phosphogluconolactonase				
11.	8a	-3.155	-3.155	-28.08	Pass
12.	6d	-3.11	-3.11	-62.44	Fail
13.	PlmIX				
14.	8a	-5.322	-5.322	-76.7	Pass
15.	6d	-5.001	-5.001	-59.89	Pass
16.	Dual specificity protein phosphatase YVH1				
17.	6d	-2.67	-2.67	-53.18	Fail
18.	8a	-2.225	-2.225	-42.49	Fail
19.	DNA-endonuclease				
20.	6d	-3.933	-3.933	-39.67	Pass
21.	8a	-3.209	-3.209	-30.54	Pass
22.	PlmV				
23.	6d	-5.977	-5.977	-55.59	Fail
24.	8a	-5.588	-5.588	-73.55	Fail
25.	Aminopeptidase N				
26.	8a	-5.029	-5.029	-58.09	Fail
27.	6d	-4.538	-4.538	-33.92	Fail
28.	Leucine aminopeptidase				
29.	8a	-3.459	-3.459	-66.2	Fail
30.	6d	-3.168	-3.168	-43.63	Fail
31.	Serine-repeat antigen protein 5				
32.	6d	-2.827	-2.827	-53.94	Pass
33.	8a	-2.769	-2.769	-44.4	Pass
34.	Falcilysin				
35.	6d	-3.789	-3.789	-44.8	Fail
36.	8a	-3.704	-3.704	-21.34	Fail
37.	Serine-repeat antigen protein 6				Fail

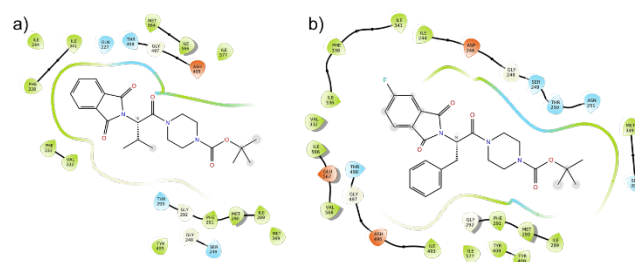


Figure 7. Schematic depiction of two-dimensional interaction maps derived from the molecular mechanics/generalized Born surface area (MM-GBSA) docking outputs against PlmIX for (a) compound **6d** and (b) compound **8a**.



Figure 8. Molecular blind docked complex of a) PlmIX-**6d**; and b) PlmIX-**8a**.

CONCLUSION

We synthesized twelve novel Pht analogs and examined their antiplasmodial efficacy on *Pf* culture. All the analogs were moderately active and exhibited no cytotoxicity on human RBCs and HepG2 cells. The most active analogs **6d** and **8a** displayed IC₅₀ values of 1.20 μM and 1.66 μM, respectively. Extensive molecular docking studies against 12 vital proteins from pool of 62 proteins indicated PlmIX as prime target of identified hits. However, these results need further validation in enzymatic experiments. Our results demonstrate the possibility of additional chemistry work to synthesize derivatives with enhanced biochemical and pharmacokinetic properties.

ACKNOWLEDGMENTS

BR thanks the Science & Engineering Research Board for the financial support (CRG/2020/005800). MB is grateful to ICMR for the senior research fellowship.

SUPPLEMENTARY INFORMATION

¹H NMR, ¹³C NMR, ADME calculations, Plot showing essential genes, Details of protein target used for docking.

Conflict of interest: Authors declare no conflict of interest.

REFERENCES AND NOTES

1. E. Fernández-Álvarez, W.D. Hong, G.L. Nixon, P.M. O'Neill, F. Calderón. Antimalarial Chemotherapy: Natural Product Inspired Development of Preclinical and Clinical Candidates with Diverse Mechanisms of Action. *J. Med. Chem.* **2016**, 59 (12), 5587–5603.
2. Y. Ma, Y. Zhu, D. Zhang, et al. Eco-friendly decarboxylative cyclization in water: Practical access to the anti-malarial 4-quinolones. *Green Chem.* **2019**, 21 (3), 478–482.
3. L.B. Arendse, S. Wyllie, K. Chibale, I.H. Gilbert. Plasmodium Kinases as Potential Drug Targets for Malaria: Challenges and Opportunities. *ACS Infect. Dis.* **2021**, 7 (3), 518–534.

4. M. De Lera Ruiz, P. Favuzza, Z. Guo, et al. The Invention of WM382, a Highly Potent PMIX/X Dual Inhibitor toward the Treatment of Malaria. *ACS Med. Chem. Lett.* **2022**, 13 (11), 1745–1754.
5. WHO. World Malaria Report 2022 - World | ReliefWeb. *World Health Organization*. 2022, p 293.
6. V. Reddy, D.J. Weiss, J. Rozier, F.O. ter Kuile, S. Dellicour. Global estimates of the number of pregnancies at risk of malaria from 2007 to 2020: a demographic study. *Lancet Glob. Heal.* **2023**, 11 (1), e40–e47.
7. A. Cohen. Role of the European Pharmacist in the Implementation of the Latest WHO Guidelines for Malaria. *Pathogens* **2023**, 12 (5), 729.
8. Poonam, Y. Gupta, N. Gupta, et al. Multistage inhibitors of the malaria parasite: Emerging hope for chemoprotection and malaria eradication. *Med. Res. Rev.* **2018**, 38 (5), 1511–1535.
9. R.W. Heidebrecht, C. Mulrooney, C.P. Austin, et al. Diversity-oriented synthesis yields a novel lead for the treatment of malaria. *ACS Med. Chem. Lett.* **2012**, 3 (2), 112–117.
10. K.J. Deane, R.L. Summers, A.M. Lehane, R.E. Martin, R.A. Barrow. Chlorpheniramine Analogues Reverse Chloroquine Resistance in *Plasmodium falciparum* by Inhibiting PfCRT. *ACS Med. Chem. Lett.* **2014**, 5 (5), 576–581.
11. R.J. Commons, J.A. Simpson, K. Thriemer, et al. The effect of chloroquine dose and primaquine on *Plasmodium vivax* recurrence: a WorldWide Antimalarial Resistance Network systematic review and individual patient pooled meta-analysis. *Lancet Infect. Dis.* **2018**, 18 (9), 1025–1034.
12. L.C. Okell, M. Cairns, J.T. Griffin, et al. Contrasting benefits of different artemisinin combination therapies as first-line malaria treatments using model-based cost-effectiveness analysis. *Nat. Commun.* **2014**, 5 (1), 5606.
13. Z.R. Lun, P.E. Ferreira, L.C. Fu. Artemisinin resistance in *Plasmodium falciparum*. *Lancet Infect. Dis.* **2014**, 14 (6), 450–451.
14. A. Mbengue, S. Bhattacharjee, T. Pandharkar, et al. A molecular mechanism of artemisinin resistance in *Plasmodium falciparum* malaria. *Nature* **2015**, 520 (7549), 683–687.
15. M. Bansal, C. Upadhyay, Poonam, S. Kumar, B. Rathi. Phthalimide analogs for antimalarial drug discovery. *RSC Med. Chem.* **2021**, 12 (11), 1854–1867.
16. A.K. Singh, V. Rajendran, A. Pant, et al. Design, synthesis and biological evaluation of functionalized phthalimides: A new class of antimalarials and inhibitors of falcipain-2, a major hemoglobinase of malaria parasite. *Bioorganic Med. Chem.* **2015**, 23 (8), 1817–1827.
17. A.K. Singh, S. Rathore, Y. Tang, et al. Hydroxyethylamine based phthalimides as new class of plasmepsin hits: Design, synthesis and antimalarial evaluation. *PLoS One* **2015**, 10 (10), 139347.
18. V. Singh, R.S. Hada, R. Jain, et al. Designing and development of phthalimides as potent anti-tubulin hybrid molecules against malaria. *Eur. J. Med. Chem.* **2022**, 239, 114534.
19. P. Kumar, A.O. Achieng, V. Rajendran, et al. Synergistic blending of high-valued heterocycles inhibits growth of *Plasmodium falciparum* in culture and *P. berghei* infection in mouse model. *Sci. Rep.* **2017**, 7 (1), 6724.
20. N. Kushwaha, D. Kaushik. Recent advances and future prospects of phthalimide derivatives. *J. Appl. Pharma. Sci.* **2016**, 159–171.
21. H. Zhang, J. Wu, J. Wang, et al. Novel Isoindolinone-Based Analogs of the Natural Cyclic Peptide Fenestin A: Synthesis and Antitumor Activity. *ACS Med. Chem. Lett.* **2022**, 13 (7), 1118–1124.
22. S. Singh, V. Rajendran, J. He, et al. Fast-Acting Small Molecules Targeting Malarial Aspartyl Proteases, Plasmepsins, Inhibit Malaria Infection at Multiple Life Stages. *ACS Infect. Dis.* **2019**, 5 (2), 184–198.
23. C.Y. Okada-Junior, G.C. Monteiro, A.C.C. Aguiar, et al. Phthalimide Derivatives with Bioactivity against *Plasmodium falciparum*: Synthesis, Evaluation, and Computational Studies Involving bc1 Cytochrome Inhibition. *ACS Omega* **2018**, 3 (8), 9424–9430.
24. A. Kumar Singh, V. Rajendran, S. Singh, et al. Antiplasmodial activity of hydroxyethylamine analogs: Synthesis, biological activity and structure activity relationship of plasmepsin inhibitors. *Bioorganic Med. Chem.* **2018**, 26 (13), 3837–3844.
25. M.A. González, J. Clark, M. Connelly, F. Rivas. Antimalarial activity of abietane ferruginol analogues possessing a phthalimide group. *Bioorganic Med. Chem. Lett.* **2014**, 24 (22), 5234–5237.
26. A. Rani, A. Sharma, J. Legac, et al. A trio of quinoline-isoniazid-phthalimide with promising antiplasmodial potential: Synthesis, in-vitro evaluation and heme-polymerization inhibition studies. *Bioorganic Med. Chem.* **2021**, 39, 116159.
27. M.N. Romanelli, D. Manetti, L. Braconi, et al. The piperazine scaffold for novel drug discovery efforts: the evidence to date. *Expert Opin. Drug Discov.* **2022**, 17 (9), 969–984.
28. P.A. Magriotis. Recent progress toward the asymmetric synthesis of carbon-substituted piperazine pharmacophores and oxidative related heterocycles. *RSC Med. Chem.* **2020**, 11 (7), 745–759.
29. A.P. Taylor, R.P. Robinson, Y.M. Fobian, et al. Modern advances in heterocyclic chemistry in drug discovery. *Org. Biomol. Chem.* **2016**, 14 (28), 6611–6637.
30. W. Trager, J.B. Jensen. Human malaria parasites in continuous culture. *J. Parasitol.* **2005**, 91 (3), 484–486.
31. A. Daina, O. Michielin, V. Zoete. SwissADME: A free web tool to evaluate pharmacokinetics, drug-likeness and medicinal chemistry friendliness of small molecules. *Sci. Rep.* **2017**, 7 (1), 1–13.
32. M. Gupta, H.J. Lee, C.J. Barden, D.F. Weaver. The Blood–Brain Barrier (BBB) Score. *J. Med. Chem.* **2019**, 62 (21), 9824–9836.
33. P.P. Sharma, S. Kumar, K. Kaushik, et al. In silico validation of novel inhibitors of malarial aspartyl protease, plasmepsin V and antimalarial efficacy prediction. *J. Biomol. Struct. Dyn.* **2022**, 40 (18), 8352–8364.
34. C. Upadhyay, S. Bhattacharya, S. Kumar, et al. Novel fluorinated piperazine based-amino acid derivatives as antiplasmodial agents: Synthesis, bioactivity and computational studies. *Chem. Biol. Lett.* **2023**, 10 (3), 543.
35. V.R. Muzykantov. Drug delivery by red blood cells: Vascular carriers designed by mother nature. *Expert Opin. Drug Deliv.* **2010**, 7 (4), 403–427.
36. F. Ding, N. V. Dokholyan. Emergence of protein fold families through rational design. *PLoS Comput. Biol.* **2006**, 2 (7), 0725–0733.
37. P. Pino, R. Caldelari, B. Mukherjee, et al. A multistage antimalarial targets the plasmepsins IX and X essential for invasion and egress. *Science* **2017**, 358 (6362), 522–528.